Ocean Dynamics (2004) 54: 266–283
DOI 10.1007/s10236-003-0077-0

Adolf Stips · Karsten Bolding · Thomas Pohlmann
Hans Burchard

Simulating the temporal and spatial dynamics of the North Sea using the new model GETM (general estuarine transport model)

Received: 30 March 2003 / Accepted: 22 July 2003

Abstract Here we present results of a 1-year realistic North Sea simulation from the new model GETM (general estuarine transport model) and assess the capabilities of this model by comparing them to model results from the well-known HAMSOM (Hamburg shelf sea and ocean model) model, in situ data from the North Sea project and satellite-derived sea-surface temperature data. The annual cycle and the spatial variability of stratification and mixing in the North Sea is simulated. It is shown that the new model is successful in reproducing the general temporal and spatial dynamics of the North Sea. The major advantages of GETM for achieving improved results in this simulation are the implementation of general vertical coordinates, of a state-of-the-art turbulence model and of higher-order advection schemes. By exploiting the full capabilities of these features a more realistic simulation could be achieved. We found that the greatest differences in the model results are produced by applying advection schemes of different complexity. Here we are able to demonstrate that better advection schemes lead to stronger horizontal gradients and stronger vertical stratification during summer. When comparing these results to measurements from the North Sea project and to satellite data, we find that these stronger gradients are more realistic. Therefore, we consider it as essential to use such high-order advection schemes if the spatial variability of estuarine or shelf seas like the North Sea is to be resolved adequately. The advanced turbulence closure scheme also contributed to more realistic simulation of the vertical stratification. Finally, general vertical coordinates better resolve the shallow regions, but are also useful for the deeper regions, as they allow a better estimation of sea-surface temperature compared to traditional σ coordinates.

Keywords Numerical modelling · Shelf seas · Sea-surface temperature

Responsible Editor: Phil Dyke

A. Stips (✉)
CEC Joint Research Centre,
Institute for Environment and Sustainability,
Inland and Marine Waters Unit,
21020 Ispra(VA), Italy
e-mail: adolf.stips@jrc.it

K. Bolding
Bolding & Burchard Hydrodynamics GbR,
Strandgyden 25, 5466 Asperup, Denmark

T. Pohlmann
Institute for Marine Research, University of Hamburg,
Troplowitzstr. 7, 22529 Hamburg, Germany

H. Burchard
Institute for Baltic Sea Research, Universität Rostock,
Seestrasse 15, 18119 Rostock, Germany

1 Introduction

The North Sea is one of the most intensively studied regions on the European Continental Shelf. This can be seen by the large number of published model studies concerning this area. The annual cycle of the thermal vertical stratification and the heat storage in the North Sea was simulated by Pohlmann (1996a,b,c,d). Further recent model studies of the North Sea area have been conducted by Delhez (1996), Holt and James (1999, 2001), Berntsen and Svendsen (1999), Holt et al. (2001) and Luyten et al. (2003).

Here we use the newly developed model GETM (general estuarine transport model) to investigate some details of the annual cycle of stratification and destratification in the North Sea. The model was especially developed for coastal and estuarine applications as it has terrain-following coordinates and it deals with drying and flooding, see Stanev et al. (2003) and Burchard et al. (2003). A detailed description can be found in Burchard and Bolding (2002). The present paper is a first attempt to assess the model performance on a much larger and deeper model area. We want to test the results for the North Sea in the period November 1988 to October 1989 against model data from the HAMSOM model

(Backhaus 1985), against measured data from the North Sea Project and against satellite sea-surface temperature measurements. For this test we allow the model to evolve with a minimum of constraints, applying relaxation of temperature and salinity only at the open boundaries. The region and time of this model simulation was dictated by the availability of data for comparing the model results to measurements from the North Sea project. Therefore the simulated period coincides with that of Holt and James (1999, 2001), comprising November 1988 until October 1989.

The NOMADS2 (North Sea model advection dispersion study) concerted action aimed at comparing model output data with measurements taken during the North Sea project monitoring programme. This should give the possibility to discriminate better between the different models and to estimate error bounds for the simulated parameters. In order to broaden the aim of the present study and to have the possibility to compare our results with results from the NOMADS2 project, we decided to select the same set of integral parameters as described by Proctor et al. (2002) for NOMADS2. The HAMSOM (Hamburg shelf sea and ocean model, Backhaus 1985) model participated in NOMADS2 and was ranked among the models which gave good and realistic results for this 1-year North Sea run, (see Proctor et al. 2002). Therefore, we decided to select HAMSOM as a representative model from the NOMADS2 comparison study.

To carry out this model comparison as realistically as possible, we decided to implement GETM on the same horizontal grid as HAMSOM and to use exactly the same initial, boundary and forcing conditions as were used for the HAMSOM NOMADS2 run. As in HAMSOM a first-order upstream scheme for tracer advection is used, we use this scheme also as basic test case for GETM. The remaining differences between the two setups are the applied turbulence scheme, the chosen vertical coordinates and, to a lesser extent, also the temporal discretisation. In HAMSOM, an algebraic turbulence model is used, whereas in GETM a two-equation turbulence closure model is implemented. Further, HAMSOM is run on geopotential coordinates, whereas GETM uses general vertical coordinates.

The third assessment will be made against satellite-derived sea-surface temperature (SST) data, which allow investigation of the spatial variability of the model data. In order to have a complete spatial coverage of the model area we used monthly AVHRR data from the NOAA/NASA Ocean Pathfinder satellite.

As for the model comparison we had to run GETM using upstream and higher-order advection schemes, we had the chance to investigate additionally how different advection schemes will influence the model results in this case. Despite the fact that many studies demonstrated the clear advantages of higher-order advection schemes, first-order schemes are still employed (Schrum 1997).

In Section 2 we present a brief description of GETM as applied to the North Sea area. Some specific details of the implementation are described in Section 3. Results for the chosen integral parameters, the selected stations and the horizontal variability are presented in Section 4. Finally, the results are discussed in Section 5.

2 General model equations

This section gives a short introduction to the GETM model equations, for specific details see Burchard and Bolding (2002).

2.1 Three-dimensional momentum equations

GETM solves the three-dimensional hydrostatic equations of motion applying the Boussinesq approximation and the eddy viscosity assumption (Bryan 1969; Cox 1984; Blumberg and Mellor 1987; Haidvogel and Beckmann 1999; Kantha and Clayson 2000). In the flux form, the dynamic equations of motion for the horizontal velocity components can be written in Cartesian coordinates as:

$$\begin{aligned}&\partial_t u + \partial_x(u^2) + \partial_y(uv) - \partial_x\left(2A_h^M\partial_x u\right)\\&\quad - \partial_y\left[A_h^M(\partial_y u + \partial_x v)\right] - fv - \int_z^\zeta \partial_x b\,dz'\\&\quad + \partial_z(uw) - \partial_z[(\nu_t+\nu)\partial_z u] = -g\partial_x\left(g\zeta + \frac{1}{\rho_0}p_0\right),\end{aligned} \tag{1}$$

$$\begin{aligned}&\partial_t v + \partial_x(vu) + \partial_y(v^2) - \partial_y\left(2A_h^M\partial_y v\right)\\&\quad - \partial_x\left[A_h^M(\partial_y u + \partial_x v)\right] + fu - \int_z^\zeta \partial_x b\,dz'\\&\quad + \partial_z(vw) - \partial_z[(\nu_t+\nu)\partial_z v] = -g\partial_y\left(g\zeta + \frac{1}{\rho_0}p_0\right)\zeta.\end{aligned} \tag{2}$$

The vertical velocity is given by the continuity equation:

$$\partial_x u + \partial_y v + \partial_z w = 0\ . \tag{3}$$

Here, u, v and w are the ensemble-averaged velocity components with respect to the x, y and z direction, respectively. The vertical coordinate z ranges from the bottom $-H(x,y)$ to the surface $\zeta(t,x,y)$ with t denoting time. ν_t is the vertical eddy viscosity, ν the kinematic viscosity, f the Coriolis parameter, p_0 is the atmospheric pressure at sea level and g is the gravitational acceleration. The horizontal mixing is parameterised by terms containing the horizontal eddy viscosity A_h^M, see Blumberg and Mellor (1987). The buoyancy b is defined as

$$b = -g\frac{\rho-\rho_0}{\rho_0}, \tag{4}$$

with the density ρ and a reference density ρ_0. The last term on the left-hand sides of Eqs. (1) and (2) are the

internal (due to density gradients) and the terms on the right-hand sides are the external (due to surface slopes and atmospheric pressure variations) pressure gradients. In the latter, the deviation of surface density from reference density is neglected (see Burchard and Petersen 1997). The derivation of Eqs. (1)–(3) has been shown in numerous publications, (see e.g. Pedlosky 1987; Haidvogel and Beckmann 1999; Burchard 2002).

The equation of state for seawater (Fofonoff and Millard 1983) is used to calculate density as a function of salinity, temperature and pressure.

In hydrostatic 3-D models, the vertical velocity is calculated by means of Eq. (3). Due to this, mass conservation and free surface elevation can easily be obtained.

2.2 Kinematic boundary conditions and surface elevation equation

At the surface and at the bottom, kinematic boundary conditions result from the requirement that the particles at the boundaries are moving along these boundaries:

$$w = \partial_t\zeta + u\partial_x\zeta + v\partial_y\zeta \qquad \text{for } z = \zeta, \tag{5}$$

$$w = -u\partial_x H - v\partial_y H \qquad \text{for } z = -H. \tag{6}$$

2.3 Dynamic boundary conditions

At the bottom boundaries, no-slip conditions are prescribed for the horizontal velocity components:

$$u = 0, \quad v = 0. \tag{7}$$

With Eq. (6), also $w = 0$ holds at the bottom. It should be noted that the bottom boundary condition Eq. (7) is generally not directly used in numerical ocean models, since the near-bottom values of the horizontal velocity components are not located at the bed, but half a grid box above it. Instead, a logarithmic velocity profile is assumed in the bottom layer, leading to a quadratic friction law.

At the surface, the dynamic boundary conditions read:

$$\begin{aligned}(\nu_t + \nu)\partial_z u &= \tau_s^x,\\ (\nu_t + \nu)\partial_z v &= \tau_s^y.\end{aligned} \tag{8}$$

The surface stresses (normalised by the reference density) τ_s^x and τ_s^y are calculated as functions of wind speed, wind direction, surface roughness etc.

2.4 Lateral boundary conditions

Boundary conditions at closed and open boundaries will be treated differently. At closed boundaries, the flow must be parallel to the boundary.

For an eastern or a western closed boundary this has the consequence that $u = 0$ and, equivalently, for a southern or a northern closed boundary it follows that $v = 0$.

At open boundaries, the velocity gradients across the boundary must vanish. For an eastern or a western open boundary this has the consequence that $\partial_x u = \partial_x v = 0$ and, equivalently, for a southern or a northern open boundary it follows that $\partial_y u = \partial_y v = 0$.

At so-called forced open boundaries, the sea-surface elevation ζ is prescribed. This is done here at the western, eastern and northern open boundary.

2.5 Transport equations for temperature and salinity

The two most important tracer equations are the transport equations for potential temperature T in °C and salinity S in PSU (practical salinity units):

$$\begin{aligned}&\partial_t T + \partial_x(uT) + \partial_y(vT) + \partial_z(wT) - \partial_z(\nu_t'\partial_z T)\\ &\quad - \partial_x(A_h^T\partial_x T) - \partial_y(A_h^T\partial_y T) = \frac{\partial_z I}{c_p'\rho_0}\ ,\end{aligned} \tag{9}$$

$$\begin{aligned}&\partial_t S + \partial_x(uS) + \partial_y(vS) + \partial_z(wS) - \partial_z(\nu_t'\partial_z S)\\ &\quad - \partial_x(A_h^T\partial_x S) - \partial_y(A_h^T\partial_y S) = 0.\end{aligned} \tag{10}$$

The term on the right-hand side of the temperature Eq. (9) is for absorption of solar radiation with the solar radiation at depth z, I, and the specific heat capacity of water, c_p'. According to Paulson and Simpson (1977), the radiation I in the upper water column may be parameterised by

$$I(z) = I_0(ae^{-\eta_1 z} + (1-a)e^{-\eta_2 z}). \tag{11}$$

Here, I_0 is the albedo-corrected radiation normal to the sea surface. The weighting parameter a and the attenuation lengths for the longer and the shorter fraction of the short-wave radiation, η_1 and η_2, respectively, depend on the turbidity of the water. Jerlov (1968) defined six different classes of water from which Paulson and Simpson (1977) calculated weighting parameter a and attenuation coefficients η_1 and η_2.

At the surface, flux boundary conditions for T and S have to be prescribed. The potential temperature is of the following form:

$$\nu_t'\partial_z T = \frac{Q_s + Q_l + Q_b}{c_p'\rho_0}, \quad \text{for } z = \zeta\ , \tag{12}$$

with the sensible heat flux, Q_s, the latent heat flux, Q_l and the longwave backradiation, Q_b. Here, bulk formulae prescribed by the NOMADS2 consortium (Proctor et al. 2002) for calculating the momentum and heat-surface fluxes due to air-sea interactions have been used.

For the surface freshwater flux, which defines the salinity flux, the difference between evaporation Q_E (from bulk formulae) and precipitation Q_P (from observations or atmospheric models) is calculated:

$$\nu_t' \partial_z S = \frac{S(Q_E - Q_P)}{\rho_0(0)}, \quad \text{for } z = \zeta \ , \tag{13}$$

where $\rho_0(0)$ is the density of freshwater at sea-surface temperature. Heat and salinity fluxes at the bottom are set to zero.

2.6 Vertical turbulent exchange

The eddy viscosity ν_t (for momentum) and eddy diffusivity ν_t' (for tracers) need to be parameterised by means of turbulence models. Such models may range from simple algebraic prescription of profiles of ν_t and ν_t' (Perrels and Karelse 1982), via zero-, one-, or two-equation models (e.g. Luyten et al. 1996) to full Reynolds stress closure models (e.g. Launder et al. 1975). In GETM, a compromise between accuracy and computational effort is made in such a way that usually two-equation models are used.

The turbulence module of the Public Domain water column model GOTM (general ocean turbulence model, see http://www.gotm.net) which has been developed by Burchard et al. (1999) is implemented into GETM. This allows for great flexibility in the choice of the turbulence model and guarantees that a well-tested state-of-the-art turbulence model is always at hand inside GETM.

The features of GOTM have been extensively reported in Burchard (2002) and the citations therein. Various comparative calculations with in-situ turbulence measurements have been carried out with GOTM, which gives some confidence into the model, see, e.g. Bolding et al. (2002), Burchard and Bolding (2001), Simpson et al. (2002) and Stips et al. (2002).

GOTM has various options for turbulence models, but only some of them have been proven to give reasonable results for vertical exchange. The research for improving turbulence models is still ongoing. Presently, better parameterisations for surface wave activity and internal wave activity are under development.

So far, the best experience inside GOTM has been made with two-equation models such as the k-ε (Launder and Spalding 1972; Rodi 1980) and the Mellor-Yamada model (Mellor and Yamada (1974, 1982) and Burchard (2001a)), both being realisations of the recently developed generic two-equation model by Umlauf and Burchard (2003).

The basic one-dimensional form of the k-ε model is the following (see Burchard and Bolding 2001):

$$\partial_t k - \partial_z \left[\left(\nu + \frac{\nu_t}{\sigma_k} \right) \partial_z k \right] = P + B - \varepsilon \ , \tag{14}$$

$$\partial_t \varepsilon - \partial_z \left[\left(\nu + \frac{\nu_t}{\sigma_\varepsilon} \right) \partial_z \varepsilon \right] = \frac{\varepsilon}{k} (c_{1\varepsilon} P + c_{3\varepsilon} B - c_{2\varepsilon} \varepsilon) \ , \tag{15}$$

with the equation for turbulent kinetic energy, (14), and for its dissipation rate ε, (15). σ_k and σ_ε denote turbulent Schmidt numbers for vertical diffusion of k and ε, respectively, and P and B are shear and buoyancy production, respectively, with:

$$P = \nu_t \left[(\partial_z u)^2 + (\partial_z v)^2 \right], \qquad B = -\nu_t' \partial_z b, \tag{16}$$

and $c_{1\varepsilon}$, $c_{2\varepsilon}$, and $c_{3\varepsilon}$ are empirical parameters.

Suitable bottom and surface boundary conditions for k and ε can be derived from the law of the wall, although modifications are needed near the surface due to breaking of surface waves (Craig and Banner 1994; Craig 1996; Burchard 2001b).

The three turbulent parameters k, ε and L are interrelated through:

$$L = c_L \frac{k^{3/2}}{\varepsilon}, \tag{17}$$

with the empirical parameter c_L.

From k and ε, the eddy viscosity and diffusivity can finally be calculated by the following relation:

$$\nu_t = c_\mu \frac{k^2}{\varepsilon}, \qquad \nu_t' = c_\mu' \frac{k^2}{\varepsilon}. \tag{18}$$

Here, c_μ and c_μ' are so-called stability functions usually depending on shear, stratification and turbulent time scale, $\tau = k/\varepsilon$.
Various sets of stability functions, which contain second-moment closure assumptions, have been suggested. The most successful in terms of comparison to laboratory and field data seems to be the closure introduced by Canuto et al. (2001), which is used in this study.

The turbulence model is coupled to the hydrodynamic model via the turbulence production terms P and B as input and the eddy viscosity and diffusivity ν_t and ν_t' as output. Furthermore, surface and bottom roughness lengths are needed for the boundary conditions inside the turbulence model. Finally, the three-dimensional model needs to store two quantities out of k, ε and L, since GOTM is a one-dimensional model which has to read in the "old" values of k, ε and L for each horizontal position. Advective transports of turbulent quantities are neglected here.

3 Specific remarks on the models

Both models solve the 3-D baroclinic shallow-water equations in the hydrostatic approximation as described in the previous section. For the horizontal discretisation, we selected spherical coordinates.

3.1 HAMSOM

The circulation model is a modified version of the shelf sea model developed by Backhaus (1985). It is a three-dimensional, baroclinic primitive equation model. Additionally, the equation of state for seawater (Fofonoff and Millard 1983) and the transport equations for temperature and salinity are employed.

In regard to scaling arguments the horizontal diffusion terms can be neglected in both transport equations, as the numerical diffusion introduced by the applied vector-upstream advection scheme is in the order of the expected physical diffusion. The vertical viscosity is parameterised using the Kochergin approach (Kochergin 1987) for the vertical turbulence closure. In this approach the vertical diffusivity is dependent on the vertical velocity gradient and the stability of the water column. In the transport equations for temperature and salinity the advective terms are formulated explicitly. Further details as well as a validation of the turbulent closure scheme can be found in Pohlmann (1996d).

3.1.1 Numerical Scheme

The equations are solved on an Arakawa-C grid in a semi-implicit form, i.e. the gravity waves and the vertical exchange and diffusion terms are treated implicitly, whereas all the other terms are formulated explicitly. For the Coriolis term a rotational matrix is applied, guaranteeing a second-order stability. In the transport equation for temperature and salinity the advective terms are formulated explicitly. For the horizontal components a selective vector-upstream algorithm is used (Backhaus 1990), while the vertical advection is calculated with the help of a component-upstream scheme. The explicit formulation in this equation causes no additional limitations of the time step due to stability considerations, because typical values of the advection velocity are of the order of $O(1\mathrm{ms}^{-1})$ which is by at least a factor of 10 smaller than the speed of the barotropic free surface waves. This means that the limiting Courant number resulting from the explicit advection approximation does not restrict the time step too rigorously. A small horizontal background diffusivity for the transports of 50 $\mathrm{m}^2\mathrm{s}^{-1}$ was applied.

To overcome the time-restrictive stability criteria of the diffusion equation the vertical diffusion of temperature and salinity is formulated implicitly in a way analogous to the vertical shear stress term in the momentum equations. The time step is 900 s. HAMSOM uses z coordinates for the vertical discretisation, which are non-equidistantly distributed. In the upper part there are ten layers of 5 m thickness each. The applied background vertical diffusivity for laminar conditions is 10^{-7} $\mathrm{m}^2\mathrm{s}^{-1}$.

At the open boundaries a zero-gradient condition for momentum is used. At inflow temperature and salinity boundary values were imposed with a relaxation time scale of 7 days. In the case of outflow from the model domain, only the component normal to the boundary of the advection velocity was considered. This so-called Sommerfeld radiation condition is described in Orlansky (1976).

3.2 GETM

For the spatial discretisation a staggered C grid is used. GETM allows the selection of different order scalar advection schemes, e.g. UPSTREAM (UP), SUPERBEE (SU) and the ULTIMATE QUICKEST (QU) scheme, which were used here for comparison. The advection schemes can be applied to transport temperature and salinity and separately also momentum can be treated with a higher-order scheme, for details see Burchard and Bolding (2002).

The turbulence scheme of GETM is chosen via the GOTM turbulence model. In this study we used the standard k-ε turbulence closure, without imposing a length limitation or background vertical diffusivity. GETM uses different time steps for the internal (macro time steps) and the external mode (micro time steps). The chosen micro time step for this setup is 60 s, the split factor is 30, which gives a macro time step of 1800 s. No background horizontal diffusion was applied. It could be argued that this is not the most appropriate approach, because of the large grid size used here and the consequent resolved subgrid mesoscale mixing; but as one aim was to look at the influence of different advection schemes, we avoided the introduction of horizontal diffusion, as this could have masked the differences between the performed simulations. The imposed boundary conditions for temperature and salinity are relaxed to the model values using a five-point sponge layer. For better resolving the shallow parts of the North Sea we decided to use general vertical coordinates with a slight zooming towards the surface and the bottom. The surface layer thickness was chosen to be 2 m overall.

3.3 Model domain and boundary conditions

3.3.1 Model domain

The model domain was chosen to coincide exactly with the setup of the HAMSOM model for the NOMADS2 model comparison study. It covers the North Sea from the channel to 61.5°N, with a horizontal resolution of about 20 km. The longitudinal grid size is $\Delta x = 20'$ and the latitudinal grid size is $\Delta y = 12'$. The bathymetry for both models is shown in Fig. 1. The grid size for both models is $58 \times 65 \times 19$ ($x \times y \times z$) points. To compare different integral parameters derived from the model output data, the so-called common area (CA) between 51°N and 57°N was selected by the NOMADS2 consortium and is also used here. The average volume of the common area for the HAMSOM model is 1.34×10^{13} m^3 and for the GETM model it is 1.44×10^{13} m^3. The difference can be explained by the use of different vertical coordinates. The z-coordinates used within HAMSOM will lead to a slight underestimation of the total volume, because the bottom-nearest layer does not always extend to the real depth.

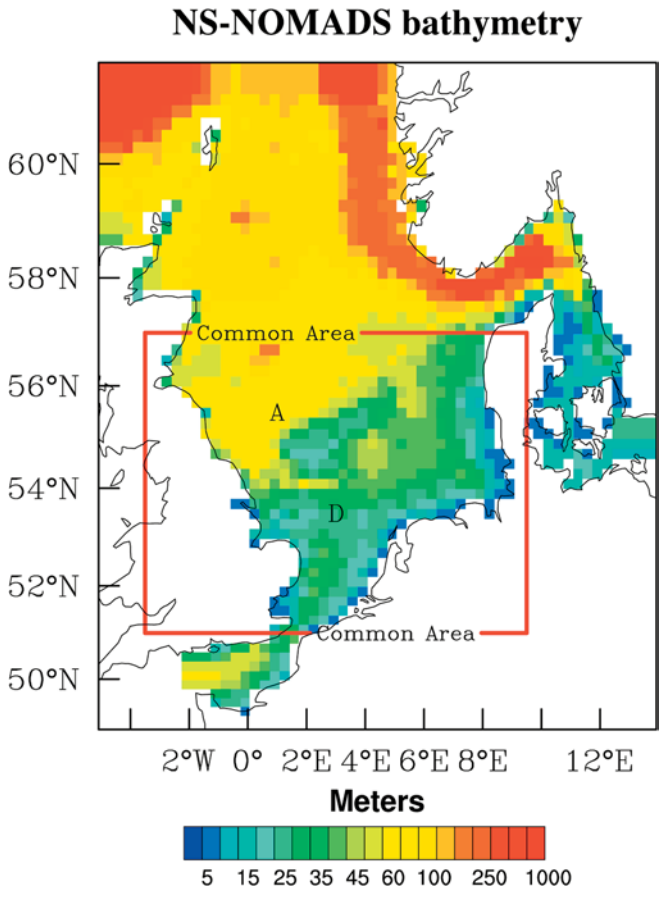

Fig. 1 Model bathymetry (depth in m) for both models of the North Sea area. The specified common area is indicated by a *red box*. The selected stations from the North Sea project are denoted by *A* (stratified) and *D* (mixed)

3.3.2 Meteorological forcing

The simulation period is November 1, 1988, to October 31, 1989. The same realistic meteorological forcing is used for GETM and HAMSOM, provided from the UK Meteorological Office. Space- and time-varying variables such as wind velocity vector, air pressure, air temperature, relative humidity and cloudiness were used to calculate surface heat and momentum fluxes. The heat flux formulae are identical for both models, so that the heat flux is practically prescribed. The 3-hourly meteorological data were interpolated onto the model grid.

3.3.3 Initial and boundary conditions

For both models and all different runs the same initial conditions were applied for water elevation, salinity and temperature. Consistent boundary values for water elevation, salinity and temperature for the 1-year realistic simulation were used. The time frequency of the tidal data is hourly. Salinity and temperature are given at monthly intervals. All these data are identical to the NOMADS2 initial and boundary dataset. For river runoff and Baltic inflow monthly mean values were used. The temperature of the freshwater inflow was assumed to be the ambient temperature.

Table 1 Characteristics of the different HAMSOM and GETM runs. The *first column* gives the RUN-Id for further reference, the *second column* the used turbulence closure, the *third column* the applied temperature and salinity advection method and the *last column* the momentum advection method

RUN-Id	Turbulence	TS adv.	M adv.
HAMSOM	Kochergin	UP	UP
GETM-UP	$k-\varepsilon$	UP	UP
GETM-SU	$k-\varepsilon$	SU	UP
GETM-SU2	$k-\varepsilon$	SU	SU
GETM-QU	$k-\varepsilon$	QU	UP
GETM-QU2	$k-\varepsilon$	QU	QU

3.4 Performed realistic 1-year simulations

For the 1-year simulation period five different GETM runs as described in Table 1 were selected. These runs comprise different turbulence closures and advection schemes with increasing degree of complexity. HAMSOM was run using the Kochergin approach for the turbulence and vector upstream advection for tracers and momentum. GETM was always used with the standard $k-\varepsilon$ two-equation turbulence closure. Three different advection schemes for tracers and momentum were tested for GETM, the first-order upwind scheme (referenced as GETM-UP), the SUPERBEE scheme by Roe (1985) (referenced as GETM-SU) and the quadratic upstream interpolation for convective kinematics with estimated stream terms by Leonard (1991) (referenced as GETM-QU). This scheme is also called the ULTIMATE QUICKEST and fulfils the condition of diminishing total variation. The major reason for using the upstream scheme was that it could be compared directly to the HAMSOM results. The runs GETM-SU2 and GETM-QU2 apply the respective higher-order advection scheme also for the advection of momentum. They are referenced in Table 1, but as the respective results differed only slightly from the results of the runs without using higher-order momentum advection, they will not be discussed in detail. It should be mentioned that this small influence of improved momentum advection, might be caused by the rather coarse grid resolution of 20 km and could be different when using smaller grid boxes.

4 Results

Results of the 1-year realistic model run using GETM are presented and compared to integral parameters from the HAMSOM model, to North Sea project data and to satellite observations.

4.1 Comparison with HAMSOM results

By the NOMADS2 consortium a set of comprehensive integral parameters that have been calculated over the common area has been proposed. We selected the following representative set of these quantities: potential energy, stratified area, kinetic energy and mean temperature. These parameters formed the basis for the model evaluation done in NOMADS2, (Proctor et al. 2002; Delhez Personal Communication 2003). We use these parameters to test the basic capabilities of the new model against results from the HAMSOM model.

4.1.1 Potential energy

The first investigated integral parameter is the total potential energy of the common area, which is presented in Fig. 2. The potential energy of the water column is defined by (in J)

$$V_s = \sum_{i,j,k} (\rho_{i,j,k} - \overline{\rho}_{i,j}) g x_3 (\Delta x_1 \Delta x_2 \triangle x_3)_{i,j,k}, \tag{19}$$

where $\overline{\rho}_{i,j}$ is the depth-mean water density at the grid point (i,j) and x_3 is the vertical coordinate, which is increasing upwards and is zero at the surface. The potential energy thus defined is zero for a well-mixed water column and negative for a stratified water column. Therefore in the following discussion the term maximum potential energy corresponds to the maximum absolute value of potential energy.

During winter both models predict a quasi-well-mixed water column. The onset of stratification occurs in both models on the same day (163). Substantial differences show up during summer stratification and autumn destratification. The largest amount of potential energy is created with the SUPERBEE (SU) scheme, whereas the UPSTREAM (UP) scheme has about 30% less potential energy during peak stratification. The maximum potential energy is about -5×10^{14} J for GETM-UP, -6×10^{14} J for HAMSOM, -6.8×10^{14} J for GETM-QU and -7×10^{14} J for GETM-SU. This larger potential energy delays the following mixing of the water column in autumn by more than 4 weeks, in better agreement with reality. It is interesting to note that during the spring restratification HAMSOM and GETM-SU agree very well. The results of GETM-QU are not shown, as they coincide practically with the GETM-SU curve.

In the NOMADS2 comparison study (Proctor et al. 2002) HAMSOM had the lowest absolute values for this 1-year simulation study, the other models ranged from -8×10^{14} J to -18×10^{14} J. Therefore it can be concluded that GETM would belong to the group of models with the overall lowest potential energy during peak stratification.

4.1.2 Stratified area

The total stratified area as part of the common area is defined as the horizontal area (Proctor et al. 2002), where the vertical density difference (maximum density–minimum density) exceeds

$$\Delta\rho_{\text{ref}} = 0.1[\text{kg m}^{-3}].$$

It is obvious from Fig. 3, that both models are completely mixed during the winter months. Further, HAMSOM and GETM-UP are destratifying fully at the end of the simulation, whereas GETM-SU remains partially stratified. In the period between day 100 and day 170 GETM-SU shows some isolated stratification events. Between day 180 and 320 HAMSOM and GETM-SU agree very well, having differences of less than 5% of the stratified area. Again, GETM-QU is not plotted in Fig. 3, as it coincides most of the time with GETM-SU.

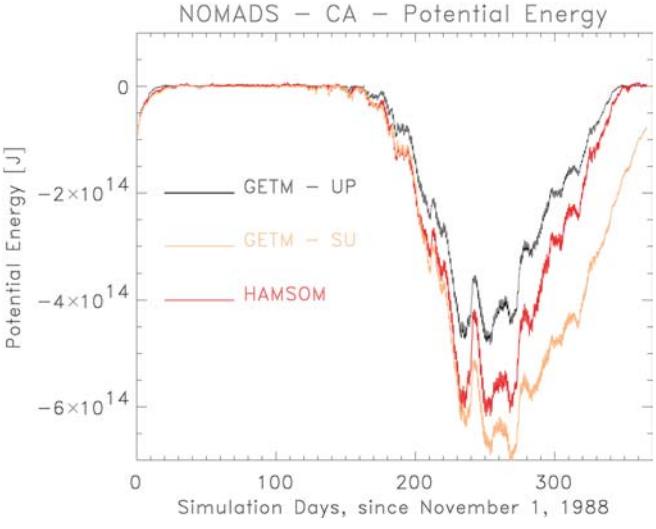

Fig. 2 Potential energy of the NOMADS common area. HAMSOM *red line*; GETM-UP *black line*; GETM-SU *yellow line*

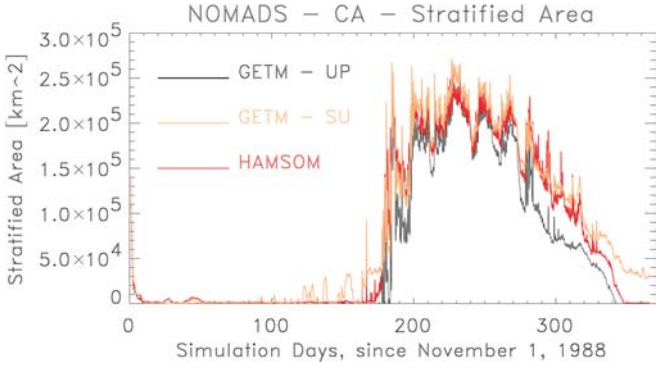

Fig. 3 Stratified area in the NOMADS common area. HAMSOM *red line*; GETM-UP *black line*; GETM-SU *yellow line*

4.1.3 Mean kinetic energy

The mean kinetic energy (MKE in m^2s^{-2}) of the common area is defined by

$$\mathrm{MKE}_m = \frac{1}{2V}\sum_{i,j,k}\left[(u_{i,j,k})^2 + (v_{i,j,k})^2\right](\Delta x_1 \Delta x_2 \Delta x_3)_{i,j,k}, \quad (20)$$

where u and v are the horizontal components of the velocity vector, V is the volume of the common area and the sum extends over all grid points inside the common domain.

The mean kinetic energy of the two models is very similar, see Fig. 4. It is evident from the figure that the MKE is mainly determined by the spring–neap tidal cycle of the North Sea, with periods of about 15 days. The minima of the MKE coincide very well, whereas HAMSOM has about 20% higher maxima in the MKE. In the NOMADS2 comparison study, HAMSOM had a kinetic energy that was in the middle range of the other models, so the same will be valid for GETM. We found no differences in the MKE for the different advection schemes, when applied only to the tracer equations. When applying the QUICKEST scheme in order to transport additionally momentum (run GETM-QU2), the MKE was increased by about 3%.

4.1.4 Average temperature

The temporal evolvement of the heat content of the common area, expressed as averaged temperature, can be seen in Fig. 5. It is defined by

$$T_{\mathrm{ave}} = \frac{1}{V}\sum_{i,j,k} T_{i,j,k}(\Delta x_1 \Delta x_2 \Delta x_3)_{i,j,k}. \quad (21)$$

The mean temperatures derived from GETM and HAMSOM follow each other relatively closely, having maximum differences of less than 0.5 K. These maximum differences appear during winter and summer. The initial temperature is roughly 9 °C, whereas the temperature at the end of the simulation is about 13 °C, which means that the average temperature increased by roughly 4 °C. An increase in temperature of this order of magnitude is seen in the North Sea measurements (Proctor et al. 2002). The used advection scheme has quasi neglectable influence on the total mean temperature of the common area. Also shown is the mean temperature of the upper 20 m and the layer from 20 m down to the bottom. Because the volumes of the upper and the lower layer are comparable, the total mean temperatures fall nicely between these two extreme temperatures. The strength of the stratification can be derived from the difference between the surface and bottom temperatures. Using higher-order advection schemes results in a stronger pronounced stratification of the water column. This stronger stratification is not caused by the applied turbulence closure, as for both GETM simulations the same turbulence closure scheme was used.

4.2 Comparison with North Sea project observations

In this section the model data are compared with observational data from a stratified and a well-mixed station (Lowry et al. 1992). These stations had been selected already by the NOMADS2 consortium in order to compare model results to CTD data. Further, we will refer to the results of the HAMSOM NOMADS2 run for the same stations.

4.2.1 Stratified station temperature

The vertical temperature field during the NOMADS2 annual simulation at a selected station A (55.5°N, 0.9°E, 68 m depth, see Fig. 1) is presented in Fig. 6. At this

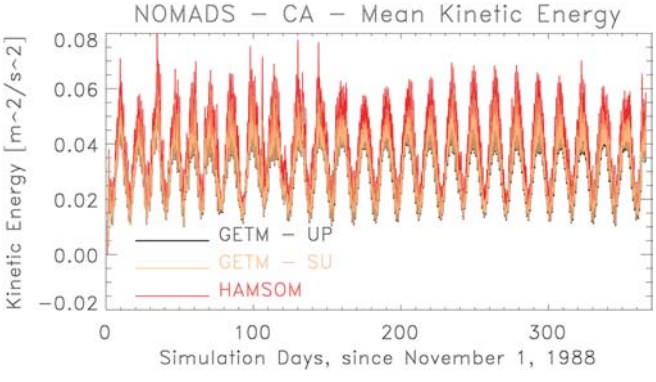

Fig. 4 Mean kinetic energy of the NOMADS common area. HAMSOM *red line*; GETM-UP *black line*; GETM-SU *yellow line*. The *black line* disappears practically behind the *yellow line*, because it was drawn first

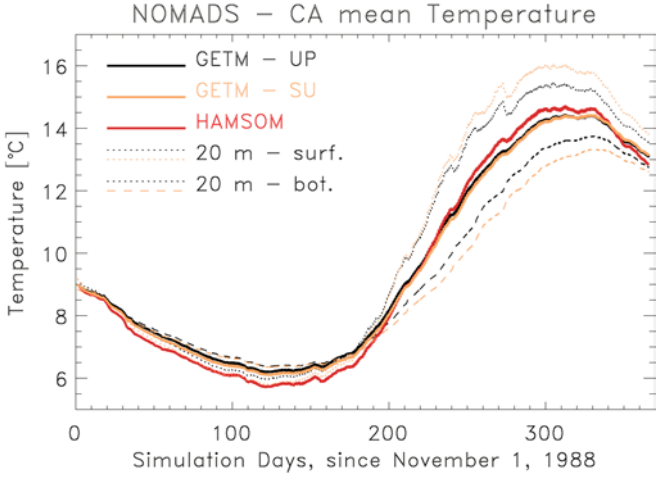

Fig. 5 Heat content of the NOMADS common area, expressed as mean temperature. The *bold lines* show the mean temperatures of the total water column, the *dotted lines* represent the upper 20 m, whereas the *dashed lines* represent the part from 20 m down to the bottom

station the water column is mixed during the winter and stratified in the summer. In the different model simulations the annual cycle of stratification and mixing is well reproduced. The results of the GETM-UP run are very similar to the HAMSOM results.

The vertical stratification during summer is more pronounced when using higher-order advection schemes; especially the thermocline is nearer to the surface and sharper, which is in better agreement with the available measurements. The surface temperatures are in good agreement with the measurements, but the water at the bottom warms up too early and too fast.

The maximum temperature (in °C) reaches 15.35 in HAMSOM, 15.23 GETM-UP and 16.51 GETM-SU, 16.53 in GETM-SU2, 16.48 in GETM-QU and 16.40 in GETM-QU2. The maximum temperature from the CTD data was 15.84 °C, but because of the low sampling frequency the real maximum temperature might have been missed in the measurements.

Comparing the model results to monthly measurements taken during that year at station A, we find that the evolution of the thermocline begins at around day 180, in accordance with the measurements. The low sampling frequency of the measurements does not allow a precise determination of this time point. The best agreement with the measurements is found in the GETM-QU simulations.

The strength of the stratification can be characterised by the temperature difference between the upper 5 m and the bottom-most 5 m. This so-called thermal stratification for station A is displayed in Fig. 7. The results for HAMSOM and GETM-UP agree quite well. Both models are well mixed until day 150, stratified between day 150 and day 340 and mixed again after day 340. HAMSOM shows a slightly larger temperature difference during the stratified phase of about 0.1 to 0.3 K more than GETM-UP. This result changes dramatically if we compare to the GETM-SU and GETM-QU output. Now during the restratification period between day 150 and day 230 GETM-QU and HAMSOM agree very well, but between day 230 and day 350 GETM-SU/GETM-QU exceeds HAMSOM by about 2 to 3 K, in better agreement with the CTD data. The maximum temperature difference between bottom and surface is 4.95 K for GETM-UP, 5.58 K for HAMSOM, 7.55 K for GETM-SU and 6.86 K for GETM-QU. The measurements gave a maximum temperature difference of 7.7 K.

4.2.2 Stratified station salinity

The small salinity variability of less than 1 PSU at the selected NOMADS2 stations makes the good simulation of salinity a challenging task. The results obtained from HAMSOM, from different GETM runs and from the North Sea project data are detailed in Fig. 8. The largest differences are in the order of 0.06–0.08 PSU.

It can be seen that the differences between the model and the measurements in salinity are rather small during most of the year, except at the end of the simulation period.

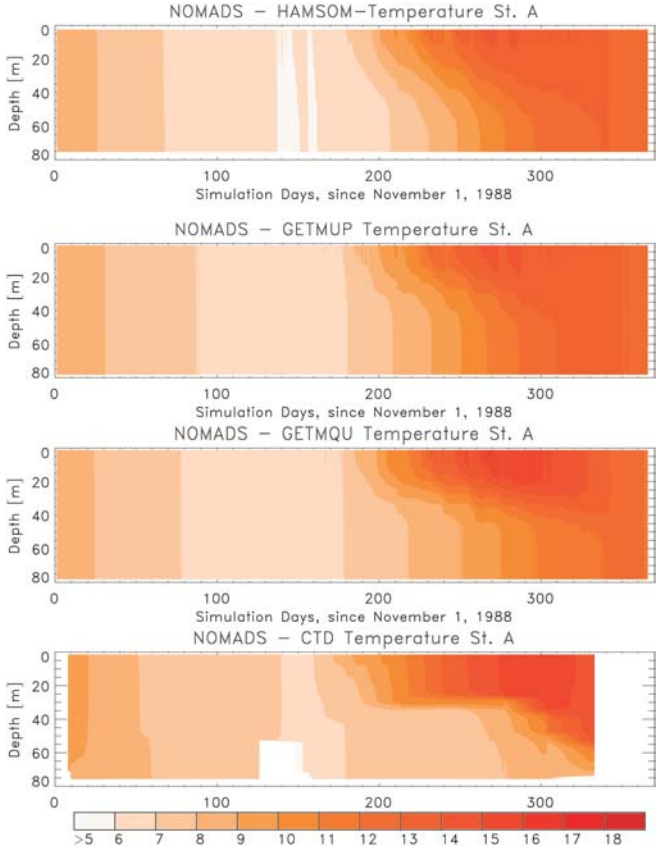

Fig. 6 Temporal evolvement of the temperature fields at the NOMADS2 station A (stratified) for different advection schemes. The *lowermost panel* shows the measurements from the North Sea project

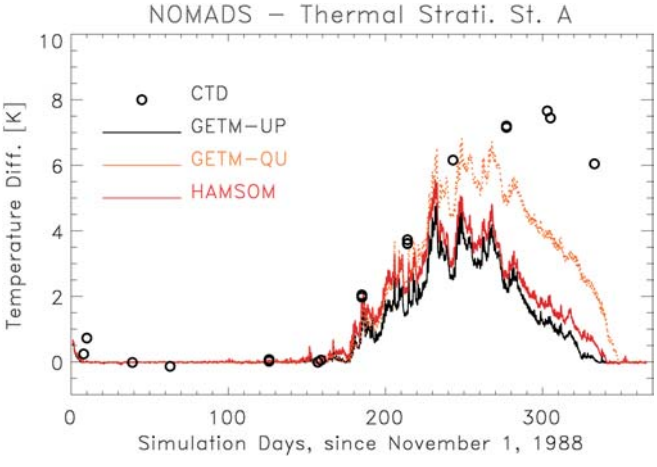

Fig. 7 Thermal stratification at station A (stratified), shown are results for the two models and different advection schemes. The *open circles* are the North Sea project data (monthly cruises)

Further we investigated the salinity difference between the uppermost 5 m and the bottom-most 5 m and compared them to CTD data, see Fig. 9. This figure reveals that the realistic simulation of salinity in the North Sea is more difficult to achieve than the hindcasting of temperature. The measurements indicate that during most of the year the salinity stratification is either stable or neutral, whereas all the simulations show during summer and especially in autumn some periods of instable saline stratification. In this case HAMSOM gives the relative best result. From the North Sea project data it can be seen that the saline stratification has a high short-term variability. This can be inferred from the appearance of two or more circles at around the same measurement time, which represent casts from the same monthly cruise. Clearly, such a short-term variability cannot be reproduced by the models, as they were forced by monthly mean values for river runoff and net precipitation.

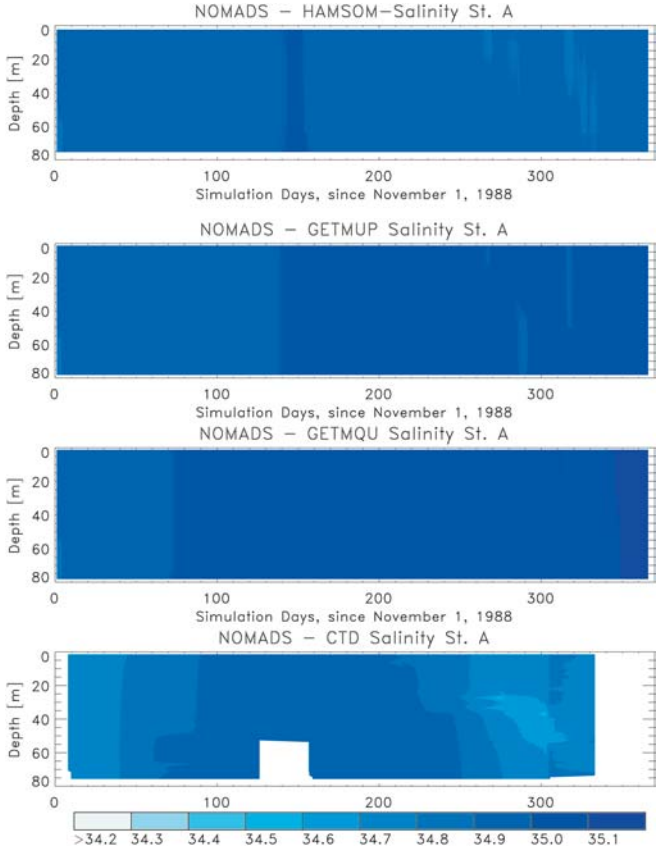

Fig. 8 Temporal evolvement of the salinity fields at the NOMADS2 station A (stratified) for the different advection schemes and measurement data from the North Sea project

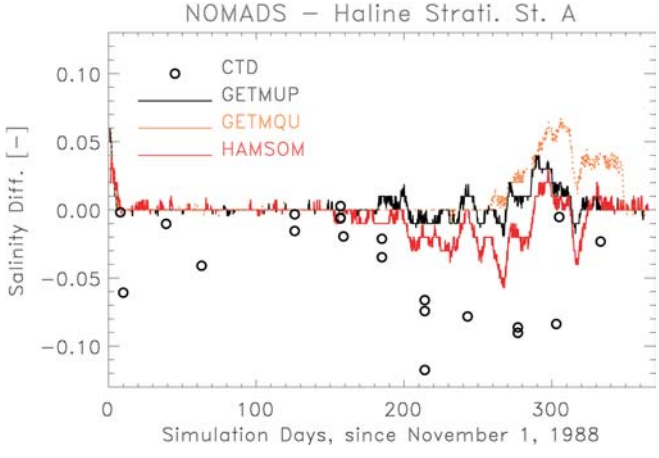

Fig. 9 Haline stratification at station A (stratified); shown are results for the different used advection schemes. The *open circles* are the North Sea project data (monthly cruises)

4.2.3 *Well-mixed station temperature*

The vertical temperature field during the NOMADS2 annual simulation at the selected station D (53.5°N, 3°E, 27 m depth, see Fig. 1) is presented in Fig. 10. During most of the year the water column is well mixed, only some minor stratification appears between day 180 and day 250. The annual cycle at this station is well reproduced by all the different advection schemes. The lowest temperature in winter (around

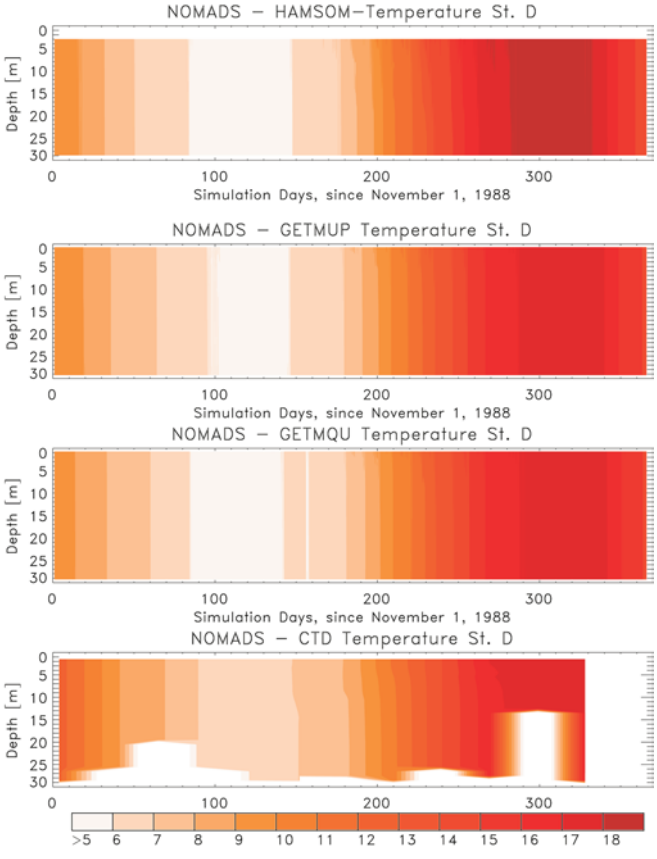

Fig. 10 Temporal evolvement of the temperature fields at the NOMADS2 station D (mixed) for different advection schemes and measurement data from the North Sea project

day 100) in the simulations is about 1 K less than in the measurements.

Minimum and maximum temperatures of the different model runs are given in Table 2. This shows that the accuracy of the simulations is in the order of 0.5 °C.

The strength of the thermal stratification at this rather mixed station D is much less compared to the stratified station A, see Fig. 11. The differences between the different models and advection schemes are quite small in this case. Until about day 150 of the simulation, the water column is completely mixed. Thereafter we see that despite the NOMADS2 classification as mixed station, stratified and non-stratified periods occur alternately during the summer. This is related to the changing position of the tidal front in the North Sea and may be also related to the spring–neap tidal cycle. The North Sea project data coincide in this case quite well with the simulations.

4.2.4 Well-mixed station salinity

The salinity range at the NOMADS2 station D is very limited. Therefore the correct simulation of salinity during an annual run is difficult to obtain. The contour plots of salinity are displayed in Fig. 12, showing the results for HAMSOM and two different tracer advection schemes compared to the data from the North Sea project. The agreement here is less satisfactory than at the stratified station A. In this case especially, even the better advection schemes show less favourable results, which suggests that the unsatisfactory simulation of the salinity field is not caused by the advection schemes used. The major reason for this behaviour might be the insufficient spatial and temporal resolution of the freshwater fluxes used.

The simulated haline stratification and the measured strength of haline stratification are about the same order of magnitude, as can be seen from Fig. 13. The typical measured and simulated salinity differences are in the order of ±0.01 PSU, showing both stable and instable stratification. Taking into account the limited accuracy of the CTD measurements, it can be concluded that the vertical strength of stratification is rather well reproduced. Contrary to the contour plot in here the results for GETM-QU agree better with the CTD data. This is probably because the absolute value of salinity cancels out, and the vertical stratification alone is better reproduced with the help of a better advection scheme.

4.3 Comparison with satellite observations

To compare the model's sea-surface temperature (SST), to satellite observations of SST, we use monthly 18-km

Table 2 Minimum and maximum temperatures (in °C) from different model runs and CTD data at station D

RUN Id	Min. temp.	Max. temp.
HAMSOM	5.38	18.95
GETM-UP	5.66	17.71
GETM-SU	5.35	18.27
GETM-QU	5.44	18.07
NSP-CTD	6.02	17.84

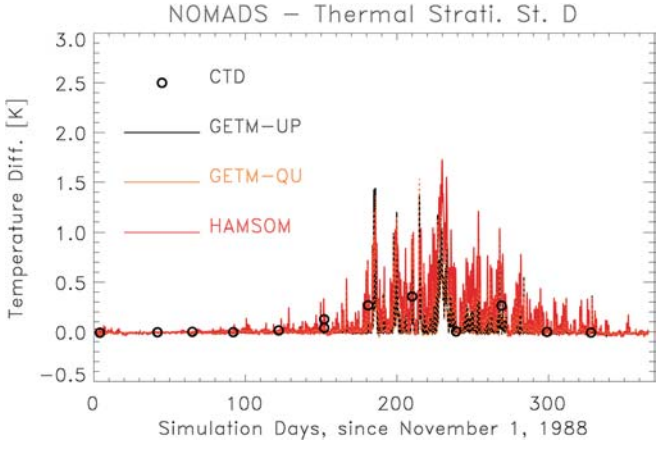

Fig. 11 Thermal stratification at NOMADS station D. Shown are results for different advection schemes and data from the North Sea project

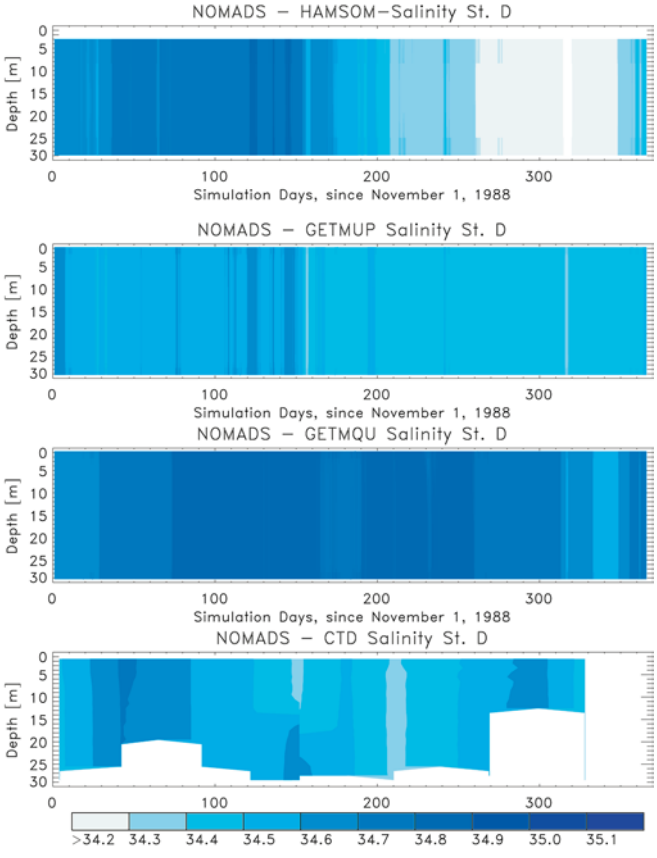

Fig. 12 Temporal evolvement of the salinity fields at the NOMADS2 station D (mixed) for the different advection schemes compared to measurements from the North Sea project

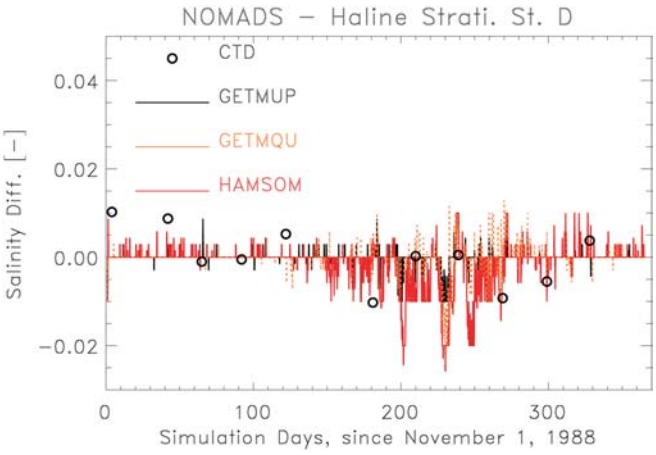

Fig. 13 Haline stratification at the well-mixed station D. Shown are results for the different used advection schemes. The *open circles* are the North Sea project data (monthly cruises)

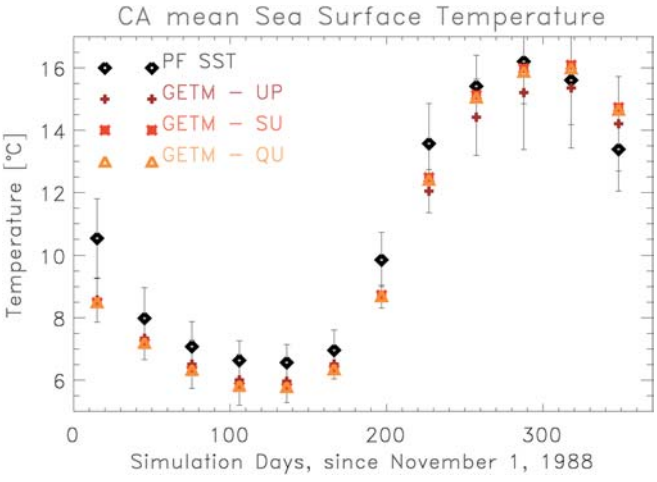

Fig. 14 Annual cycle of the monthly mean SST for the NOMADS2 common area region, including their rms deviations. PF SST are the satellite-derived SST, whereas the other three datasets are from the different GETM runs

AVHRR data from the NOAA/NASA Ocean Pathfinder satellite, see http://podaac.jpl.nasa.gov/sst. The 18-km data were chosen, as they have a horizontal resolution similar to the models. The accuracy of the satellite SSTs is supposed to be in the order of about 0.5 K, (Annan and Hargreaves 1999).

4.3.1 Mean sea-surface temperature

In order to investigate the annual cycle of SST, we calculated the mean SST and rms deviations in the common area from the monthly satellite data. The same was done for the monthly mean data of the runs GETM-UP, GETM-SU and GETM-QU. The results of these calculations are shown in Fig. 14. The temperature during the model initialisation was obviously too low, as the satellite SST is about 2 K higher than the modelled SSTs in November 1988. During the following winter months until April 1989 both temperatures agree to within 0.5 K. During the warming up of the North Sea from April to August 1989 the satellite SST exceeds the model SST by about 1 K, and showing finally a reversed behaviour during the cooling in autumn 1989. As can be seen by the indicated errors bars using the rms deviations, all monthly mean values fall within the distance of the rms deviation. The rms deviations vary from about 0.4 K in April/May to about 1.8 K in August/September. The SSTs from all different model runs are practically the same during the winter period. In the summer GETM-SU and GETM-QU are still equal, whereas GETM-UP has an SST about 0.5 K smaller.

4.3.2 Spatial variability of SST

The composite mean SST for the AVHRR data in January 1989 and February 1989 are shown in Fig. 15 together with the model results. The respective data for the summer months July and August 1989 are shown in Fig. 16. These figures show the overall model domain, but the focus for the comparisons remains on the common area, indicated by the red lines. The model has some success in reproducing the large-scale features of the satellite SST during the year. This concerns the appearance of colder water in the central North Sea during winter and the general south–north temperature gradient in the southern North Sea.

The satellite images show generally more small-scale variability than the model results. The results of GETM-UP are especially smoothed compared to those from GETM-QU. This can be best seen when comparing the images from August 1989 with each other. We can find here surface temperatures of more than 18 °C near to the Dutch coast in the AVHRR data and GETM-QU results, but not in GETM-UP. Very cold coastal waters during January 1989 and February 1989 are more restricted to the German coastal zone, as is also seen in the respective satellite data.

Compared to what is described in Holt and James (2001) we find that the seasonal dynamics in the Norwegian Trench is not that much underestimated by our model. Holt and James (2001) stated that the underestimation in their case was caused by the use of σ coordinates, which lead to rather large layer thicknesses at the deeper parts. As we used general vertical coordinates having a quasi-constant uppermost layer thickness of about 2 m, this problem could be avoided in the simulation.

Clearly, in this study the model results are very much dependent on the boundary conditions used, which are far from being optimal (Proctor et al. 2002) for a realistic study, but were chosen in order to be equal for all NOMADS2 participants. In view of this additional handicap we consider the results of the temporal spatial dynamics as satisfactory. The

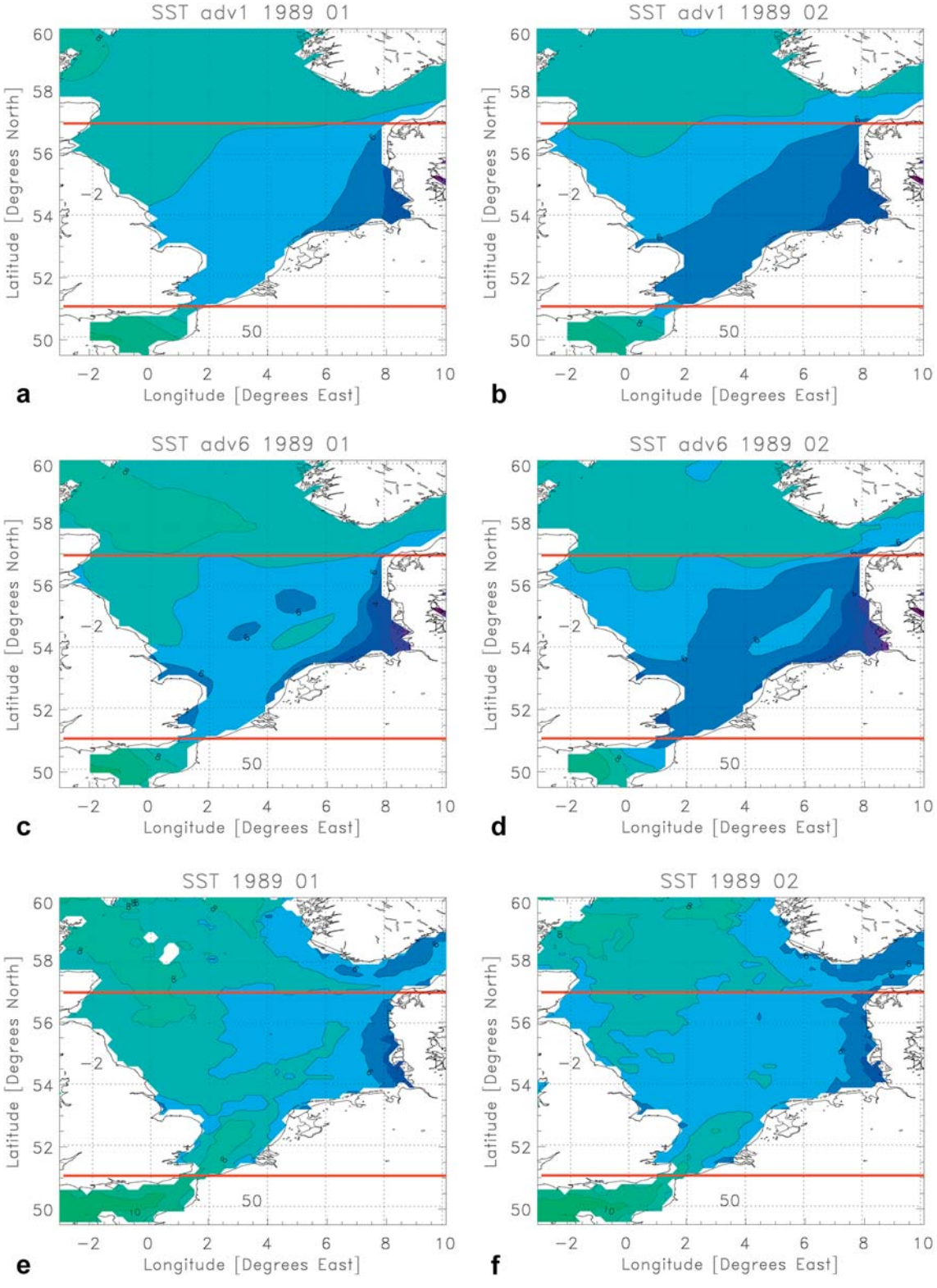

Fig. 15 Monthly mean SST from GETM-UP (*upper panel*), GETM-QU (*middle panel*) and NOAA Pathfinder satellite (*lower panel*) for the months January and February 1989

better-resolved spatial variability, when using the same grid size for both runs, again favours the use of higher-order advection schemes.

4.3.3 Detailed spatial variability

Here we present two snapshots of daily SST values, in order to compare more detailed GETM results with satellite-derived temperatures. The sea-surface temperature simulated with GETM-QU and the

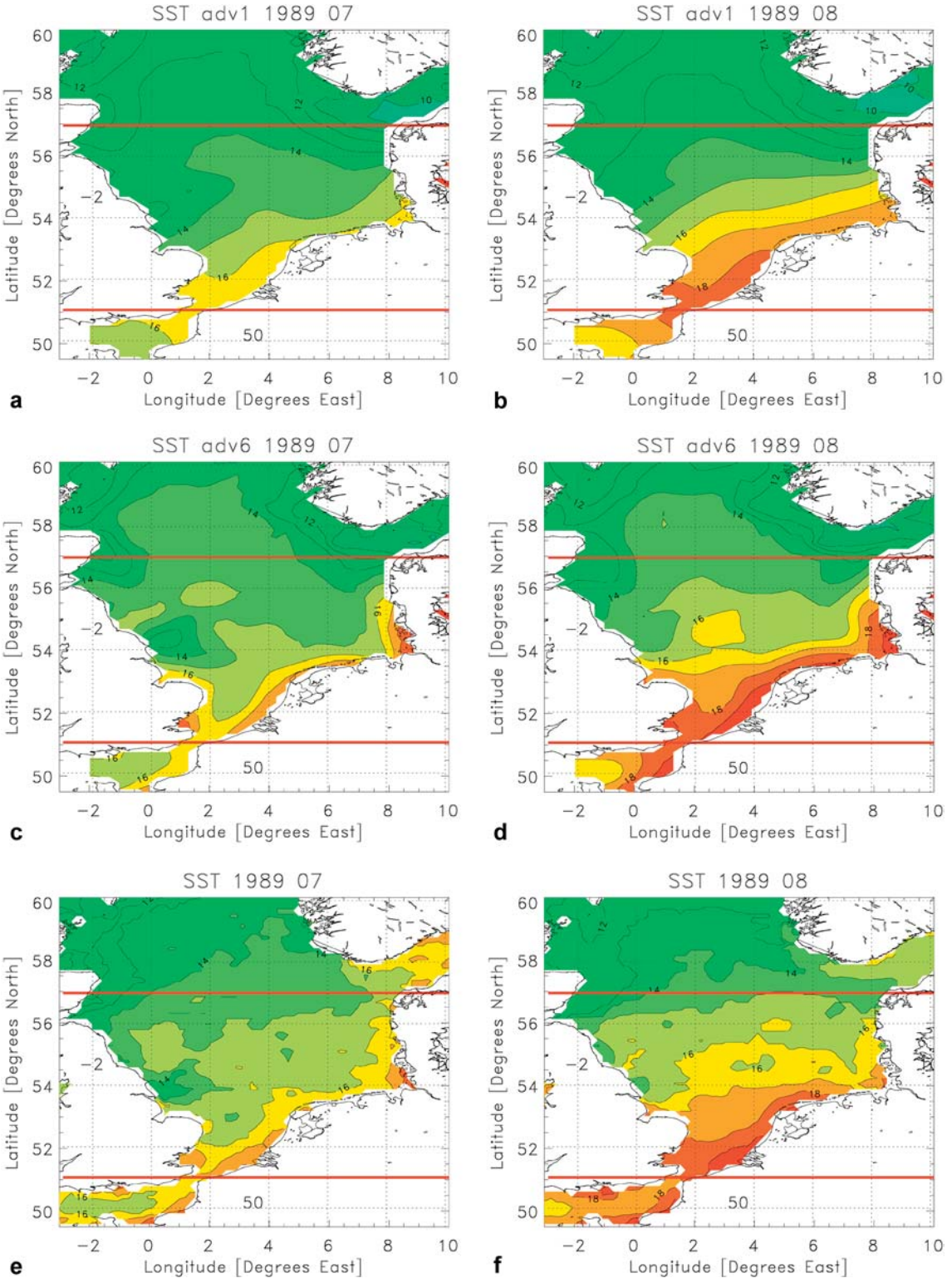

Fig. 16 Monthly mean SST from GETM-UP (*upper panel*), GETM-QU (*middle panel*) and NOAA Pathfinder satellite (*lower panel*) for the months July and August 1989

respective satellite data for July 05 are shown in Fig. 17.

The reason for selecting 5 July, 1989, was that this was the only cloudless day during all the summer months 1989, so that a nearly complete night-time satellite SST image was available for comparison. The second-best coverage, but having at the same time stronger horizontal gradients, was obtained on 20 August, 1989. The model results and the satellite SSTs are displayed in Fig. 18. Still not even the whole common area is cloud-free; unfortunately, especially the area near

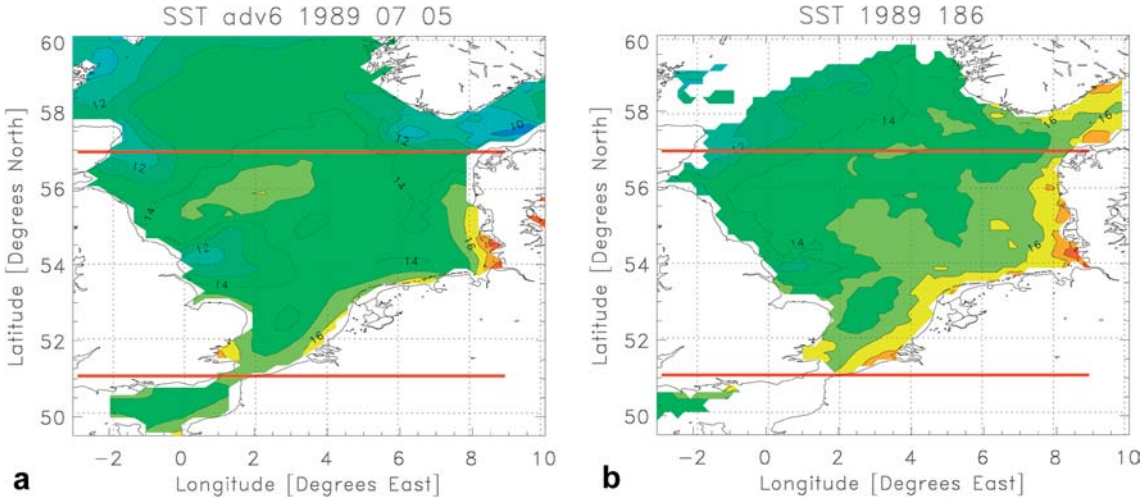

Fig. 17 Sea-surface temperature simulated by GETM using QUICK-EST tracer advection at 05 July, 1989 (*upper panel*) and the corresponding satellite data (*lower panel*, day 186)

to the German coast is not covered in the image from August. The general appearance of decreasing temperatures from up to about 18 °C in the southern North Sea down to about 13 °C at about 57°N is seen in the satellite SST and in the model data. The horizontal gradient in the satellite SST is smaller than in the model data.

Outside our region of interest the model shows up-welling in the Skagerrak area, which seems not to be present in the satellite's SST. Clearly with only two single snapshots available for comparison we cannot expect detailed coincidence of the two SST datasets.

Fig. 18 Sea-surface temperature simulated by GETM using QUICK-EST tracer advection, 20 August, 1989 (*upper panel*), and the corresponding satellite data (*lower panel*, day 232). Same colours were used as in Fig. 17

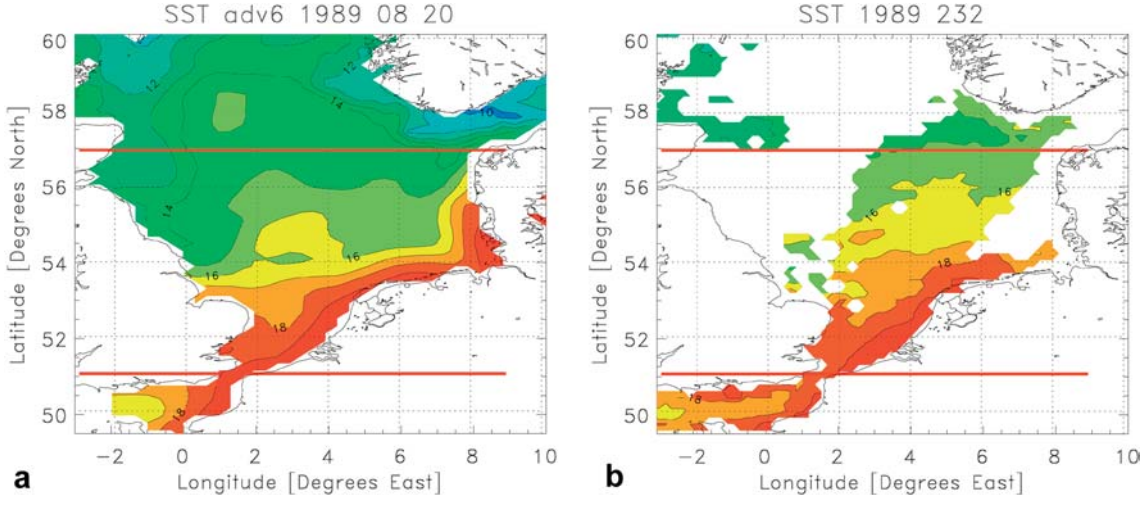

5 Discussion

5.1 Model comparison

The model comparison was based on a set of integral parameters developed by the NOMADS2 consortium. We found that GETM agrees for most of the investigated parameters very well with the HAMSOM results. This confirms that GETM reproduces the basic dynamics of the North Sea well.

The annual cycle of stratification and destratification is described by the potential energy, the stratified area and the mean temperature. These parameters demonstrate the well-known fact that the North Sea is completely mixed during winter. Stratification begins to develop in early May and reaches a maximum in July/August. The simulation of the annual cycle of the heat content in the common area gave realistic results. The temperature difference summer to winter is about 8 °C, in good agreement with the depth-mean data of all CTD stations from the North Sea project, (Holt and James 1999). It further provided evidence for the fact that during 1989 the North Sea had a positive temperature

anomaly, as the final simulated mean temperature of the common area was about 4 °C higher than the initial temperature.

The much stronger wind and pressure fields during the winter cause much higher and more variable volume transports through the investigated east–west sections. The magnitude of the simulated volume transport through the Dover Strait seems to be far too small in all model runs. Partially this might be caused by the boundary conditions at the Channel, but to point to a real reasoning seems not to be possible in the framework of this study.

In recent years, a number of model comparisons have been made, see, e.g MEDMEX for the Mediterranean Sea, NOMADS1 and NOMADS2 for the North Sea and DAMME-NAB for the Atlantic. The basic idea behind these comparisons was to run a number of models under similar conditions with respect to the input data (e.g. bathymetry, initial and boundary data and meteorological forcing). Then the model results were evaluated by comparing different integral parameters. The outcome of most of these studies was that quite large deviations exist between the different models. These deviations are attributed to specific model details such as, e.g. the turbulence closure used, the advection methods, the boundary conditions or the slightly different model domains. Excluding some of these differences by choosing an almost identical setup definitely improves the agreement of the model results, as shown in this study. The simulation results are improved compared to HAMSOM when we are using the advanced features of GETM.

In our opinion, the ability to discriminate models by the use of such integral parameters seems to be limited, also E.J.M. Delhez, personal communication (2003).

5.2 North Sea project data

It is not a priori clear that using only an improved numerics but the same forcing will give results closer to the measured values. This was also shown by the NOMADS2 comparison study (Proctor et al. 2002), in which some models using advanced advection/turbulence schemes did not give significantly better results than HAMSOM. To test model results against station data, which represent instantaneous measurements at a fixed point, is always a challenging task. The stations were arbitrary selected by the NOMADS2 consortium to represent contrasting dynamical behaviour during the annual simulation. The annual cycle of cooling and warming was well reproduced at both stations. This is true especially for the surface temperatures. It can be noted that using better turbulence closure and advection scheme within GETM will give better results compared to HAMSOM (see Fig. 7). As HAMSOM belonged to the group of the most realistic models during the NOMADS2 comparison of model to North Sea project data, this confirms that GETM is able to reproduce the temperature and salinity observations at least as well as, if not better than, the best models for the North Sea.

Less favourable was the simulation of the sharpness of the thermocline and the bottom temperature at the stratified station A. Most likely the model overestimates the vertical diffusion, which will smear out the thermocline and transports too much heat downward. This is expressed in Figs. 6 and 7, where we can see that the smaller thermal stratification is mainly caused by the higher bottom temperatures. Therefore, it is not surprising that the temperature simulation at the well-mixed station D is reproducing the measurements very well, even when using UPSTREAM advection. In this case, the diffusive behaviour of the UPSTREAM advection does not matter, because there are practically no vertical gradients to be diffused.

Even more difficult seems to be the prognostic treatment of salinity in the North Sea, as it is influenced by inflow of freshwater from several large rivers as well as by the inflow from less saline water from the Baltic Sea and the difference between evaporation and precipitation. Especially at station D, several times less saline water bodies, probably caused by river outflow, were found. These events could not be reproduced by the model. Similar problems with the salinity simulation were reported by the NOMADS2 consortium (Proctor et al. 2002); but it must be considered that the forcing for the freshwater fluxes was far from being optimal. Instead of using monthly mean values as done in the NOMADS2 study, at least daily freshwater fluxes must be prescribed in order to achieve a more realistic simulation of salinity. This underlines that with present-day models and forcing data we are still not able to reproduce accurately the dynamics at an arbitrarily selected station. This has, of course, to do with the uncertainty of the initial and boundary conditions as well as that of the forcing data, which can lead to increasing deviations from reality with time. Further, it must be considered that we in fact compare point-like measurements to mean values from the selected grid box. In order to allow for quantitave comparisons, a sampling strategy for the measurements should be developed, which would provide real temporal and spatial averages over selected grid boxes.

5.3 AVHRR SST data

The internal Rossby radius in the North Sea ranges from about $\sim$3 km in river plumes to about $\sim$20 km in the Norwegian Trench. Therefore the model setup used could not resolve details of the baroclinic features in the North Sea.

The occurrence of river plumes, confined to the coasts, can be seen in the respective plots of sea-surface temperature. How much they are trapped to the coast depends mainly on the tracer advection scheme used. Lower-order schemes that are more diffusive reduce horizontal gradients considerably.

The simulated annual cycle of SST in the North Sea agrees rather well with the satellite data. The specific choice of an uppermost layer which is at almost constant depth below the surface helps to compare the model results to satellite data. This represents a clear advantage compared to the use of traditional σ coordinates.

The monthly mean values of simulated and satellite SST show principally the same features. The imposed initial temperature was below the satellite SST values, therefore in the winter months the simulated SSTs are colder than the measured ones, but showing a similar structure. During the summer months the agreement is improved and especially the results from the run GETM-QU give some confidence in the simulations.

We undertook some effort to compare daily satellite SSTs with model results. Unfortunately, we must acknowledge that this is practically not feasible; because of the northern location of the North Sea, there are too many days obscured by clouds. Therefore it seems to be necessary to rely in such comparisons on at least eight daily or monthly SST averages. The disadvantage of this approach is, clearly, that any synoptic variability which is in the order of 3–4 days in that area will be filtered out. To test the short-term response of such 3-D models against satellite SSTs will therefore not be that easy in such northern areas.

6 Conclusions

The agreement between the model results obtained from simulations of the North Sea dynamics using GETM and HAMSOM is quite promising and especially much better than some differences found between different models during the NOMADS2 study. This is valid despite the different turbulence closures applied for HAMSOM and GETM, but using a similar advection scheme. Using higher-order advection schemes the results differ considerably, leading to an improved simulation of the North Sea dynamics by GETM.

Higher-order advection schemes lead not only to stronger horizontal gradients as often assumed, but also to a much stronger pronounced vertical stratification in the North Sea. When comparing these results to measurements from the North Sea project and to satellite data, we find that these stronger gradients are more realistic.

Holt and James (2001) stated that the use of the Mellor–Yamada–Galperin (Mellor and Yamada 1982; Galperin et al. 1988) level 2.5 turbulence closure scheme did not give satisfactory results, as it provides an inadequate treatment of statically unstable layers. Therefore they finally decided not to use the turbulence closure but preferred a simple convective adjustment procedure. However, such a convective adjustment scheme is not energy-conserving and is therefore a rather unphysical way of dealing with this problem. We could demonstrate that the use of a $k-\varepsilon$ turbulence closure scheme is well justified and leads to improved simulation results. Contrary to the conclusions of Holt and James (2001), we find that the use of advanced turbulence closures is necessary for a more realistic simulation of the vertical stratification, resulting in a shallower and sharper pycnocline.

Comparing the relative influence resulting from turbulence parameterisation and from advection scheme implementation on the results, it seems that for this North Sea simulation the influence of the advection scheme dominates that of the turbulence closure used. Therefore we consider it essential to use such high-order advection schemes, if the horizontal and vertical variability of estuarine or shelf seas like the North Sea is to be resolved adequately.

If the forcing is correct, then present-day models should reproduce the observed salinity patterns in a statistically correct sense down to the model resolution. To improve such simulations in order to match reality better, especially the forcing and boundary conditions must be more adequate for the desired task (e.g. prescribing daily freshwater fluxes).

The use of general vertical coordinates leads to a more detailed representation of shallow regions and therefore improves the simulation especially there, compared to z-coordinate models, where eventually only one or two layers would remain for describing the complex dynamics in the shallow coastal zone. Further, they are also advantageous compared to traditional σ coordinates, as they allow a fine resolution of the near-surface layer, practically independent of the actual water depth.

In this study GETM demonstrated some of its capabilities for a more realistic simulation of shelf sea areas. In summary, the combination of improved features, as general vertical coordinates, state-of-the-art turbulence closure model and total variation diminishing–higher order advection schemes gave better results for the NOMADS2 North Sea data, compared to other models participating in this study.

Acknowledgements The authors of this paper are grateful to the NOMADS2 consortium, which undertook great efforts in order to establish a basis for model intercomparisons in the North Sea area. Especially we wish to thank Roger Proctor the coordinator of NOMADS2 and Morten Skogen for supplying the model bathymetry and the open-boundary data. The meteorological data are provided by the UK-Met Office. Part of this work was done under the project ECOWAT (2121) in framework programme FP6.

References

Annan JD, Hargreaves JC (1999) Sea-surface temperature assimilation for a three-dimensional baroclinic model of shelf seas. Continental Shelf Res 19: 1507–1520

Backhaus JO (1985) A three-dimensional model for simulation of shelf sea dynamics. Dt Hydrogr Z 38: 165–187

Backhaus JO (1990) On the atmospherically induced variability of the circulation of the Northwest European Shelf Sea and related phenomena – a model experiment. In: Davies AM (ed), Modeling marine systems. vol I. p CRC Press, Boca Rota, Florida, 93–134

Berntsen J, Svendsen E (1999) Using the SKAGEX dataset for evaluation of ocean model skills. J Mar Sys 8: 313–331

Blumberg AF, Mellor GL (1987) A description of a coastal ocean circulation model. In: Heaps NS (ed) Three-dimensional ocean models. American Geophysical Union, Washington, DC pp 1–16.

Bolding K, Burchard H, Pohlmann T, Stips A (2002) Turbulent mixing in the northern North Sea: a numerical model study. Continental Shelf Res 22: 2707–2724

Bryan K (1969) A numerical model for the study of the world ocean. J Comp Phys 4: 347–376

Burchard H (2001a) Note on the $q2$ equation by Mellor and Yamada (1982). J Phys Oceanogr 31: 1377–1387

Burchard H (2001b) Simulating the wave-enhanced layer under breaking surface waves with two-equation turbulence models. J Phys Oceanogr 31: 3133–3145

Burchard H (2002) Applied turbulence modelling in marine waters, Lecture notes in earth sciences. Vol 100 Springer, Berlin, Heidelberg, New York

Burchard H, Bolding K (2001) Comparative analysis of four second-moment turbulence closure models for the oceanic mixed layer. J Phys Oceanogr 31: 1943–1968

Burchard H, Bolding K (2002) GETM, a general estuarine transport model. Scientific documentation. Technical report, European Commsission, Ispra

Burchard H, Bolding K, Villarreal MR (2003) Three-dimensional modelling of estuarine turbidity maxima in a tidal estuary. Ocean Dynamics

Burchard H, Bolding K, Villarreal MR (1999) GOTM–a general ocean turbulence model. Theory, applications and test cases. Technical Report EUR 18745 EN, European Commission

Burchard H, Petersen O (1997) Hybridisation between σ and z coordinates for improving the internal pressure gradient calculation in marine models with steep bottom slopes. Int J Numer Meth Fluids 25: 1003–1023

Canuto VM, Howard A, Cheng Y, Dubovikov MS (2001) Ocean turbulence I: one-point closure model. Momentum and heat vertical diffusivities with and without rotation. J Phys Oceanogr 31: 1413–1426

Cox MD (1984) A primitive equation, 3-dimensional model for the ocean. Technical Report 1, Geophysical Fluid Dynamics Laboratory, University of Princeton, Princeton NJ

Craig. PD (1996) Velocity profiles and surface roughness under breaking waves. J Geophys Res 101: 1265–1277

Craig PD, Banner ML (1994) Modelling wave-enhanced turbulence in the ocean surface layer. J Phys Oceanogr 24: 2546–2559

Delhez EJM (1996) Reconnaissance of the general circulation of the North-Western European Continental Shelf by means of a three-dimensional turbulent closure model. Earth Sci Rev 41: 3–29

Fofonoff NP, Millard. RC (1983) Algorithms for computation of fundamental properties of seawater. UNESCO Technical Papers in Marine Science. 44: 1–53

Galperin B, Kantha LH, Hassid S, Rosati A (1988) A quasi-equilibrium turbulent energy model for geophysical flows. J Atmosph Sci 45: 55–62

Haidvogel DB, Beckmann A (1999) Numerical ocean circulation modelling. Series on environmental science and management, Vol 2. Imperial College Press, London

Holt JT, James ID (1999) A simulation of the southern North Sea in comparison with measurements from the North Sea project. part 1: Temperature. Continental Shelf Res 19: 1087–1112

Holt JT, James ID (2001) An s coordinate density evolving model of the northwest European continental shelf, 1. Model description and density structure. J Geophys Res 106: 14015–14034

Holt JT, James ID, Jones JE (2001) An s coordinate density evolving model of the northwest European continental shelf, 2. Seasonal currents and tides. J Geophys Res 106: 14035–14053

Jerlov NG (1968) Optical oceanography. Elsevier, New York

Kantha LH, Clayson CA (2000) Numerical models of oceans and oceanic processes. International geophysics series. Vol 66 Academic Press, New York

Kochergin VP (1987) Three-dimensional prognostic models. In: Heaps NS (ed) Three-dimensional ocean models, American Geophysical Union, Washington, DC pp. 201–208.

Launder BE, Reece GJ, Rodi W (1975) Progress in the development of a Reynolds-stress turbulence closure. J Fluid Mech 68: 537–566

Launder BE, Spalding DB (1972) Mathematical models of turbulence. Academic Press, New York

Leonard BP (1991) The ULTIMATE conservative difference scheme applied to unsteady one-dimensional advection. Comput Meth Appl Mech Eng 88: 17–74

Lowry RK, Cramer RN, Rickards LJ (1992) North Sea project. Technical report, British Oceanographic Data Centre NERC CD-ROM

Luyten PJ, Deleersnijder E, Ozer J, Ruddick KG (1996) Presentation of a family of turbulence closure models for stratified shallow water flows and preliminary application to the Rhine outflow region. Continental Shelf Res 16: 101–130

Luyten PJ, Jones JE, Proctor R (2003) A numerical study of the long- and short-term temperature variability and thermal circulation in the North Sea. J Phys Oceanogr 33: 3756–3772

Mellor GL, Yamada T (1974) A hierarchy of turbulence closure models for planetary boundary layers. J Atmosph Sci 31: 1791–1806

Mellor GL, Yamada T (1982) Development of a turbulence closure model for geophysical fluid problems. Rev Geophys 20: 851–875

Orlansky I (1976) A simple boundary condition for unbounded hyperbolic flows. J Comp Phys 21: 251–269

Paulson CA, Simpson JJ (1977) Irradiance measurements in the upper ocean. J Phys Oceanogr 7: 952–956

Pedlosky J (1987) Geophysical fluid mechanics, 2ne ed. Springer, Berlin Heildeberg New York

Perrels PAJ, Karelse M (1982) A two-dimensional, laterally averaged model for salt intrusion in estuaries. Technical Report Tech. Rep. 262, Waterloopkundig Laboratorium, Delft Hydraulics, Delft, Netherlands

Pohlmann T (1996a) Calculating the annual cycle of vertical eddy viscosity in the North Sea with a three-dimensional circulation model. Continental Shelf Res 16: 147–161

Pohlmann T (1996b) Calculating the annual cycle of vertical eddy viscosity in the North Sea with a three-dimensional circulation model. Continental Shelf Res 16: 147–161

Pohlmann T (1996c) Calculating the development of the thermal vertical stratification in the North Sea with a three-dimensional circulation model. Continental Shelf Res 16: 163–194

Pohlmann T (1996d) Predicting the thermocline in a circulation model of the North Sea, part I. Model description, calibration and verification. Continental Shelf Res 16: 131–146

Proctor R, Damm P, Delhez E, Dumas F, Gerritsen H, de Goede E, Jones JE, de Kok J, Ozer J, Pohlmann T, Rasch P, Skogen M, Sorensen JT (2002) North Sea model advection dispersion study 2. Assessments of model variability, nomads-2: final report. Technical Report MAS3-CT98-0163, Commission of the European Countries, Brussels, Belgium

Rodi W (1980) Turbulence models and their application in hydraulics. Technical report, International Association for Hydraulic Research Delft, The Netherlands

Roe PL (1985) Some conributions to the modeling of discontinuous flows. Lect Notes Appl Math 22: 163–193

Schrum C (1997) Thermohaline stratification and instabilities at tidal mixing fronts: results of an eddy-resolving model of the German Bight. Continental Shelf Res 17: 689–716

Simpson JH, Burchard H, Fisher NR, Rippeth TP (2002) The semi-diurnal cycle of dissipation in a ROFI: model-measurement comparisons. Continental Shelf Res 22: 1615–1628

Stanev EV, Wolff JO, Burchard H, Bolding K, Flöser G (2003) On the circulation in the East Frisian Wadden Sea: numerical modeling and data analysis. Ocean Dynamics 53: 27–51

Stips A, Burchard H, Bolding K, Eifler W (2002) Modelling of convective turbulence with a two-equation k-ε turbulence closure scheme. Ocean Dynamics 52: 153–168

Umlauf L, Burchard H (2003) A generic length-scale equation for geophysical turbulence models. J Mar Res 61: 235–265